Effect of Isocyanate-Modified Fumed Silica on the Properties of Poly(butylene succinate) Nanocomposites

Jung Seop Lim,[1] Sung Min Hong,[1] Dong Kook Kim,[2] Seung Soon Im[1]

[1]*Department of Fiber and Polymer Engineering, College of Engineering, Hanyang University, Seoul 133-791, Korea*
[2]*Department of Chemistry, Hanyang University, Ansan, Korea*

Received 15 April 2007; accepted 1 September 2007
DOI 10.1002/app.27532
Published online 5 December 2007 in Wiley InterScience (www.interscience.wiley.com).

ABSTRACT: Using the grafting method on a silica surface with PBS molecules, we prepared novel poly(butylene succinate) (PBS)/silica nanocomposites to enhance dispersibility and interfacial adhesion between silica particles and the PBS matrix, and also investigated the effects of silica-*g*-PBS on the PBS matrix using differential scanning calorimetry, thermogravimetric analysis, transmission electron microscopy, a tensile testing machine, and rheometry. The thermal stability, mechanical properties, and rheological properties of PBS nanocomposites containing silica-*g*-PBS was remarkably improved because of the surface characteristics of the silica grafted with PBS molecules, which provided good compatibility and dispersion. © 2007 Wiley Periodicals, Inc. J Appl Polym Sci 107: 3598–3608, 2008

Key words: poly(butylene succinate); nanocomposite; silica; *in situ* polymerization

INTRODUCTION

Poly(butylene succinate) (PBS) is a biodegradable aliphatic polyester synthesized by the polycondensation of 1,4-butanediol with succinic acid.[1–4] PBS has several interesting properties, including biodegradability, melt processability, and chemical resistance, which gives rise to wide potential applications.[5,6] However, other properties of PBS pose shortcomings, such as insufficient stiffness, low-melt strength and viscosity, and poor mechanical and thermal properties.

The nanocomposite is an effective way of improving these drawbacks and widening its application. Furthermore, they have merits when compared with conventional polymer composites, such as lightweight, transparency, and easier processability. Consequently, organic polymer-based nanocomposites are considered as next-generation materials.[7,8]

In the preparation of these nanocomposites, the dispersion of inorganic particles on a nanometer level and the compatibility between it and the polymer matrix are the most critical factors.[9] However, it is difficult to disperse nanoparticles in polymeric matrix homogeneously because of the strong tendency of nanoparticles to agglomerate, which is caused by the poor interaction between the hydrophilic nanoparticles and hydrophobic polymer matrix. To improve the interfacial interaction between inorganic particles and polymer matrix, many studies have attempted to convert the hydrophilic particle surface into a hydrophobic surface in the nanocomposites.[10–14]

Among them, the surface of nanoparticles grafted with polymer exhibits more hydrophobic property due to the nature of the grafting polymers, which may improve the compatibility between the polymer matrix and inorganic nanoparticles. In addition, the entanglement between the grafting polymers is known to enhance the interfacial interaction substantially.[12,15]

In this study, by grafting method, we sought to improve the dispersibility of silica and the interfacial interaction between silica particles and the PBS matrix in a PBS nanocomposite. First, to provide silica with functional groups, an isocyanate group was introduced on the silica surface using hexamethylene diisocyanate (HDI). Then, the functionalized silica particles were grafted with PBS molecules using *in situ* polymerization. This novel PBS nanocomposites may be anticipated that the compatibility between the grafted PBS and silica can be enhanced markedly, leading to the enhancement of physicochemical properties for PBS. The thermal and mechanical properties and dynamic rheological behavior of the nanocomposite were investigated to confirm the effects of grafting PBS molecules on the nanocomposite.

EXPERIMENTAL

Materials

Hydrophilic silica (Aerosil® 300) was obtained from Degussa (Düsseldorf, Germany). It has a specific

Correspondence to: S. S. Im (imss007@hanyang.ac.kr) or D. K. Kim (dkkim@hanyang.ac.kr).

Contract grant sponsor: Korea Science and Engineering Foundation; contract grant number: R01-2006-000-10489-0.

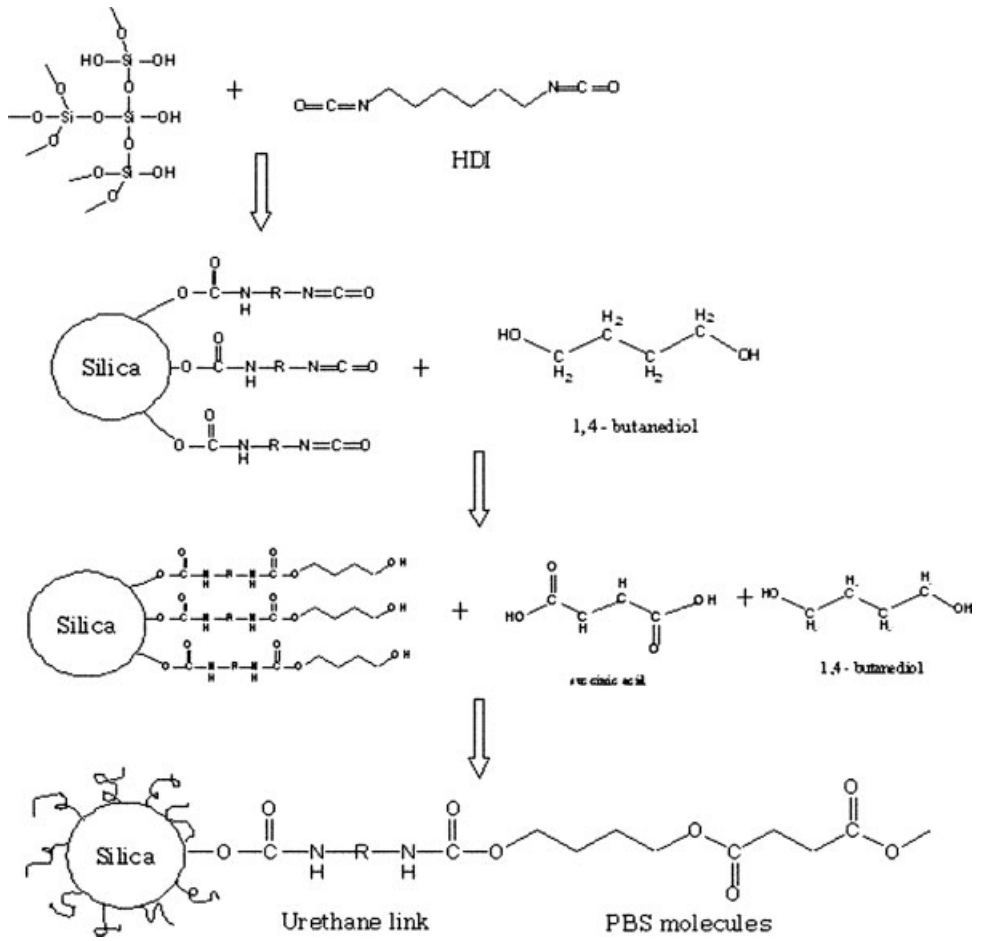

Scheme 1 Reaction scheme for PBS nanocomposites containing silica-*g*-PBS.

surface area of 300 ± 30 m^2 g^{-1} and an average primary particle size of 7 nm. 1,4-Butanediol (99%), succinic acid (99%), titanium (IV) isobutoxide (97%), HDI, and dibutyltin dilaurate were purchased from Aldrich Chemical (Milwaukee, WI) and used without further purification. Hydrophilic silica was used after drying for over 24 h in a vacuum oven.

Modification of the silica particles

Five grams of silica were suspended with stirring in 100 mL of toluene in a 500-mL round flask. An excess of HDI (5 mL) was then added to the dispersion. Several drops of dibutyltin dilaurate were introduced to the mixture as the catalyst. The mixture was stirred at 30°C under a nitrogen atmosphere for 24 h. The modified silica was obtained as slurry after centrifugation at 6000 rpm for 20 min. The slurry was washed with tetrahydrofuran (THF), and then redispersed and recentrifuged several times to remove the unreacted HDI. The solvent in the slurry was removed completely under vacuum. The resulting powder was dried in a vacuum oven at 40°C for over 24 h before characterization.

Preparation of PBS nanocomposites

The PBS nanocomposites containing unmodified and modified silica (0.5, 2.0 wt %) was prepared using *in situ* polymerization, applying conventional two-step polymerization. Modified silica was first dispersed in 1.2 mol 1,4-butanediol, using an ultrasonic homogenizer for 30 min. Then 1,4-butanediol slurry was heated to 90°C with stirring under a nitrogen atmosphere for 1 h. Afterward, the slurry was mixed with 1-mol succinic acid and 0.03 wt % titanium (VI) butoxide, and the temperature was increased to 190°C slowly with mechanical stirring. Finally, esterification was carried out for 3.5 h continuously removing the water formed. The polycondensation reaction was carried out at 235°C under a vacuum below 0.1 Torr until a sudden rise in torque occurred (2–3.5 h). The reaction scheme for the PBS nanocomposite containing silica-*g*-PBS is briefly shown in Scheme 1.

Separation of silica powder from the nanocomposites

For the quantitative determination for the extent of the covalently attached isocyanate groups per silica

particle and the degree of grafting for PBS molecules, the silica powder grafted with PBS molecules was separated from the nanocomposites by using centrifugation method. First, the prepared nanocomposites (5 g) were diluted with the 50 mL chloroform solution. Afterward, the dilute solution was separated by centrifugation machine (MICRO 22R) with speed of 6000 rpm. The obtained silica powder was redispersed and recentrifuged more than five times to remove free PBS molecules, which cannot be reacted with the silica particles. Finally, the obtained samples were dried in a vacuum at around 30°C for 24 h before the detailed analysis.

Characterization of the modified silica particles and PBS nanocomposites

To verify the chemical structure of the modified silica particles and nanocomposites, Fourier transform infrared (FTIR) analysis was conducted using a Nicolet 760 Magna-IR spectrometer (Nicolet-Magna, Madison, WI).

Thermogravimetric analysis (TGA) was used to determine the amount of the grafting polymer on the surface of the silica particles and to investigate the thermal stability of the nanocomposites. TGA was performed under an air purge at a heating rate of 5°C min^{-1} using a Pyris 6 thermal analyzer (PerkinElmer, Wellesley, MA).

The inherent viscosity of the pure PBS and PBS/silica nanocomposites were determined by using a Cannon–Ubbelohde microviscometer (Cannon Instrument, State College, PA). The measurement was done on the material from which silica was removed. For example, 2.00 g of the nanocomposite sample were dissolved in 100-mL chloroform with a concentration of 0.2 g dL^{-1}. After cooling to room temperature, the mixture was centrifuged at 5000 rpm for 20 min and then supernatant was carefully separated and was filtered by PTFE membrane filter. The inherent viscosity of samples was calculated from:

$$\eta_{rel} = \frac{t}{t_0} = \frac{\rho}{\rho_0} \quad \eta_{inh} = (\ln \eta_{rel})/C$$

where t_0, ρ_0: flow time and viscosity of the solvent; t, ρ: flow time and viscosity of the solvent; C: concentration of the solution.

The observation of the dispersibility of silica particles on the PBS matrix in the nanocomposites was carried out using transmission electron microscope (TEM; model TACNAI200; FEI, Hillsboro, OR). Ultra-thin films of the nanocomposites were prepared by solution casting. A carbon-coated mica sheet was dipped into a 0.1 wt % solution of nanocomposites and dried at room temperature. Then, the ultra-thin film supported by carbon layer was detached from the mica sheet onto a water surface, and picked up on a copper grid. The specimen on the grid was shadowed with platinum (Pt) to increase the image contrast and calibrate electron diffraction patterns. The shadow angle was $\tan^{-1}(1/3)$.

The thermal properties of the nanocomposites were measured using a TA instrument. To remove the previous thermal history, all the samples were first heated at 150°C for 5 min and then a second scan of the heating and cooling run was performed at a rate of 10°C min^{-1}.

To determine the mechanical properties of PBS/silica nanocomposites, films were prepared using a hot press at 150°C with the holding pressure of 6000 psi and the holding time of 5 min. The fabricated films were quenched in cold water and dried at 40°C for the overnight. Afterward, dried films were cut in the shape of dog-bone with 6 cm × 1 cm. Mechanical tests were conducted with a tensile testing machine (Instron 4465; Instron, Norwood, MA) at a crosshead speed of 20 mm min^{-1} at room temperature.

The rheological properties of the nanocomposite melts were measured using an advanced rheometric expansion system (ARES; Rheometric Scientific, Piscataway, NJ) with parallel plate geometry. The frequency was varied from 0.05 to 500 rad s^{-1} with a 12.5-mm diameter parallel plate with a 1.0-mm gap at 150°C.

RESULTS AND DISCUSSION

Characterization of the modified silica particles

Figure 1 shows the FTIR spectra of the (a) original silica particles, (b) silica-HDI obtained after grafting

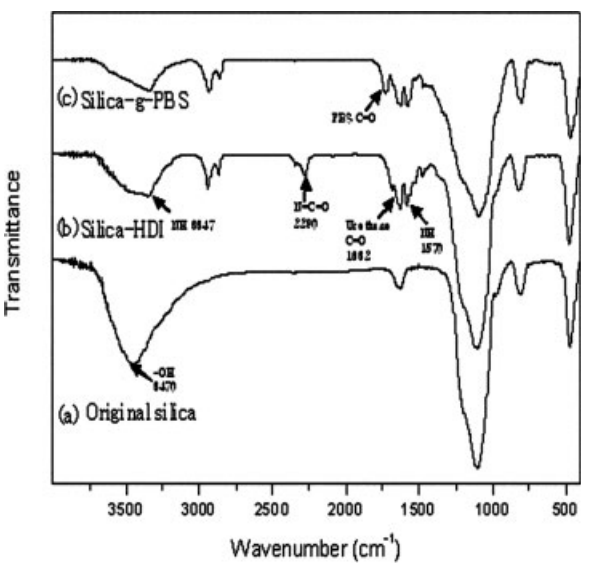

Figure 1 FTIR spectra of silica particles.

HDI to the silica surface, and (c) silica-*g*-PBS obtained after reacting the pendant HDI on the silica surface with PBS molecules. In the original silica particles, strong and broad peaks at 3470 cm^{-1}, reflecting the intramolecular hydrogen-bonded silanol hydroxyl groups and near 1100 cm^{-1}, which may attribute to the Si—O vibration, are assigned, respectively.[16] As for silica-HDI, C=O stretching peak at 1632 cm^{-1} and an amide N—H vibration peak at 1570 cm^{-1} are observed, which corresponds to the urethane bond. Besides, a peak, N—H stretching, is assigned at 3347 cm^{-1}[17] and a new peak attributable to isocyanate groups, is found at 2290 cm^{-1}.[18] These results suggest that HDI was successfully introduced on the silica particles.

Compared with the hydroxyl group of original silica, the hydroxyl band of silica-HDI shifts to a lower wavenumber and its peak occurs near 3436 cm^{-1} with a reduced intensity. These results support that the intramolecular hydrogen bonding in original silica is weaker, as a result of an incorporation of HDI group within the hydroxyl group in the silica particles. However, unique peaks, which are related to the crosslinking of silica particles or intraparticle reaction, cannot be observed in the IR spectra. On the other hand, in the case of silica-*g*-PBS, the peak of the NCO group disappeared, meanwhile the C=O stretching peak of PBS molecules appeared at 1726 cm^{-1} in the spectra. This indicates that the —NCO group of silica-HDI reacted with the —OH group of the PBS molecules during *in situ* polymerization, producing the complete silica-*g*-PBS.

Figure 2 shows the TGA curves of the original silica particles, silica-HDI, and silica-*g*-PBS. For the original silica particles, about 3% weight loss was observed as a result of the separation of physically bound water. For silica-HDI, the approximately 16.5% weight loss occurred because of the thermal decomposition of the HDI moieties. The extent of the covalently attached isocyanate groups (NCO group nm^{-2}) was determined from the TGA data. Since 1.2 g silica-HDI was used to prepare the nanocomposite, 0.198 g HDI was obtained from the weight loss of the silica-HDI. The mole value of the HDI can be obtained from the amount of HDI divided by its molecular weight, and this value was about 1.18 mmol g^{-1}. Then, the number of NCO groups per nm^2 of the silica surface was calculated using the equation as follows:

$$\text{NCO group per nm}^2 = \frac{n_{\text{HDI}} \times N_A}{A \times 10^{18}}, \qquad (1)$$

where n_{HDI} is the number of moles of HDI on the silica surface, N_A is Avogadro's number, and A is the specific surface area of silica particles. The number of isocyanate groups on the silica surface was about 2.0 NCO nm^{-2}.

For the silica-*g*-PBS, an approximately 53.8% weight loss is expected from the thermal decomposition of the grafted PBS molecules. The amount of grafted PBS molecules can be calculated from this weight loss. The extent of grafting was confirmed as the percentage of grafting by the following equation:[19]

$$\text{Percentage of grafting (\%)} = \frac{\text{Grafted PBS (g)}}{\text{Used silica particles (g)}} \times 100. \qquad (2)$$

Here, the silica particles used and grafted PBS molecules can be determined from the TGA curve of silica-*g*-PBS. The percentage of grafted PBS molecules is about 124%. As a result, the IR spectra and TGA results strongly suggest that an isocyanate group was introduced on the surface of the silica particles by the reaction of HDI with silanol groups on the silica surface, and the modified silica particles also chemically bonded with the PBS molecules after *in situ* polymerization.

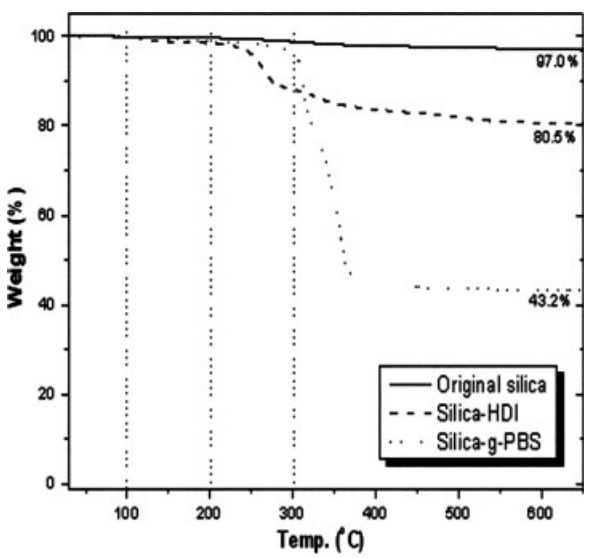

Figure 2 TGA curves of silica particles.

TABLE I
Sample Code, Reaction Time, and IV Value

Sample code	Reaction time (h)		[η]
	Esterification	Polycondensation	
Neat PBS	3.5	2.5	0.759
S05	3.5	3	0.794
S20	3.5	3.5	0.764
G05	3.5	3.5	0.808
G20	3.5	3.5	1.018

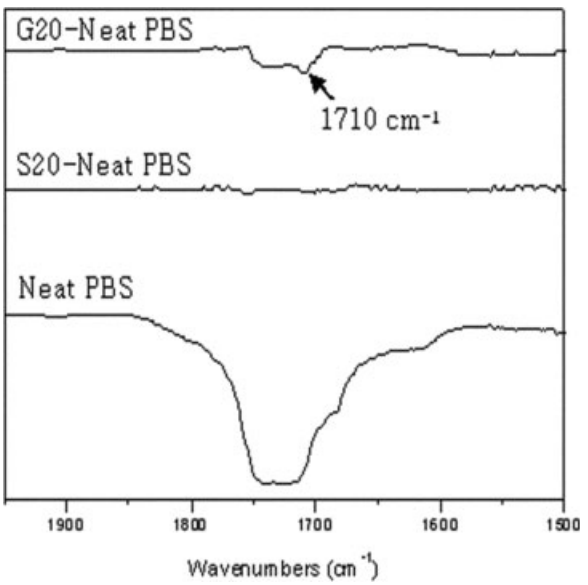

Figure 3 FTIR spectra of PBS nanocomposites: G20-neat PBS, S20-neat PBS, and neat PBS.

Characterization of the PBS nanocomposites

Reaction time and intrinsic viscosity

To identify the influence of grafting on *in situ* polymerization for the nanocomposites, the intrinsic viscosity (IV) was determined. Table I shows the sample code, reaction time, and IV data for all the PBS nanocomposites. In the sample codes, S and G denote PBS nanocomposites containing original silica particles and silica-*g*-PBS, respectively. The number following S or G is the fraction of silica in the PBS nanocomposites by weight. As shown in Table I, in the case of S05 and S20, the value of IV was similar to that of neat PBS regardless of the silica content. On the other hand, the IV of the G nanocomposites increased with the silica content and this value was definitely higher than neat PBS, indicating that relative to the unmodified silica, the modified silica may influence strongly the degrees of polymerization of PBS. This phenomenon may be explained that the grafting PBS molecules on the silica particles operates as an active site, which can improve the degree of polymerization, generating the enhancement of the molecular weight of PBS.

FTIR spectra

We checked the IR spectra of neat PBS, PBS/unmodified silica, and PBS/modified silica nanocomposites, respectively. Except the characteristic bands of PBS (ester bond, 1264 cm^{-1}; O—H, 3600–3400 cm^{-1}; C—H, 2941 cm^{-1}; C=O, 1728 cm^{-1};

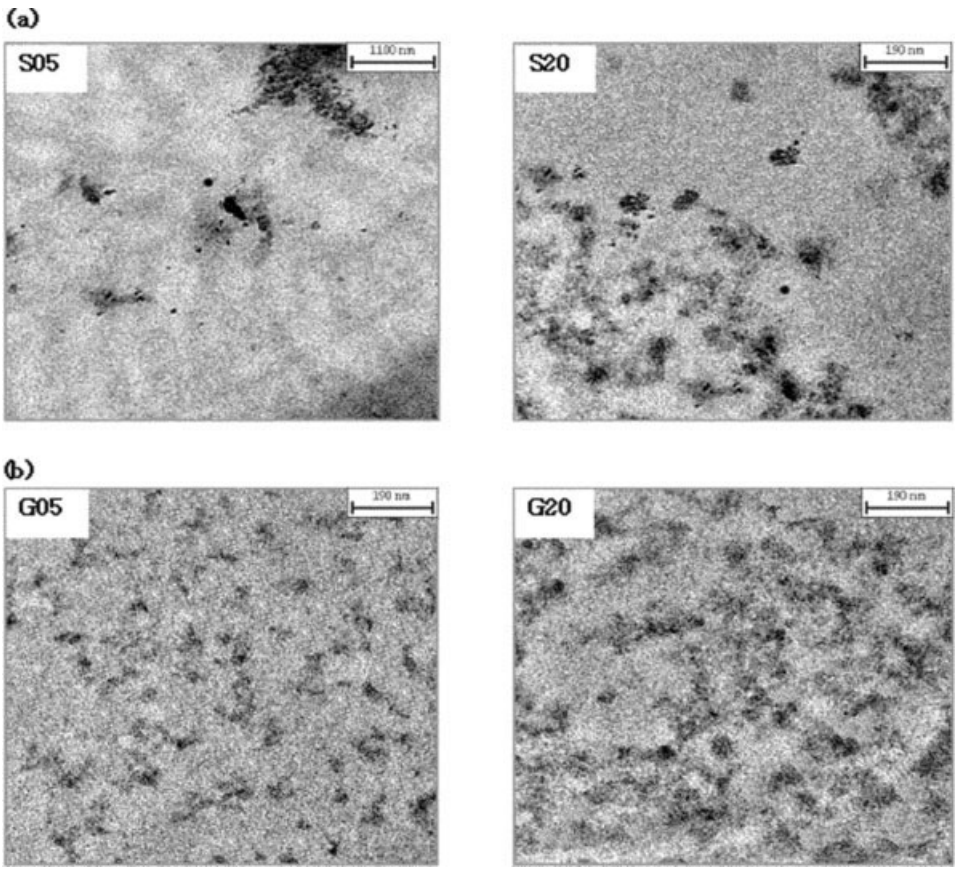

Figure 4 TEM micrographs of PBS nanocomposites: (a) S nanocomposites and (b) G nanocomposites.

TABLE II
Thermal Stability and Thermal Properties of PBS Nanocomposites

Sample	T_c (°C)	T_m (°C)	$\Delta H_{f,m}$ (J/g)	ΔT (°C)	$T_D{}^2$ (°C)	$T_D{}^{20}$ (°C)
Neat PBS	69.0	115.0	71	46.0	264	318
S05	72.3	115.0	69	42.7		
S20	76.1	115.0	65	38.9	273	319
G05	69.0	115.0	68	46.0		
G20	75.7	115.0	64	39.3	273	340

C—O, 1140 cm^{-1}),[20] there were no new peaks which may be influenced by the addition of silica, indicating that PBS/silica nanocomposites were successfully fabricated without crosslinking or intraparticle reaction of silica (data not shown).

To verify the existence of specific interaction between PBS and silica particles, the FTIR spectrum of neat PBS, S20, and G20 was normalized using the unchanged peaks, and then the S20 and G20 spectra were subtracted from the background spectrum of neat PBS; these results are shown in Figure 3. The S20-neat PBS had no characteristic peak, indicating that there is no interaction or chemical bonds created between the original silica particles and the PBS molecules. Interestingly, in the case of the G20-neat PBS, additional peak can be assigned at about 1710 cm^{-1} when compared with neat PBS.[18] On the whole, if specific hydrogen bond is formed between the carbonyl group of polyester and the functional group of other materials, some modification near this carbonyl group can be detected. For example, the wavenumbers of carbonyl group may be shifted[21,22] or new carbonyl groups near the major carbonyl group can be created.[23,24] Based on this, this new peak at 1710 cm^{-1} can be thought to be a powerful evidence that the carbonyl group of PBS molecules interacts with the —NHCO— groups of urethane between silica particles and PBS molecules, giving rise to the formation of hydrogen bonds.

Dispersibility

The dispersibility of silica particles on the PBS matrix in the nanocomposites was investigated using TEM;

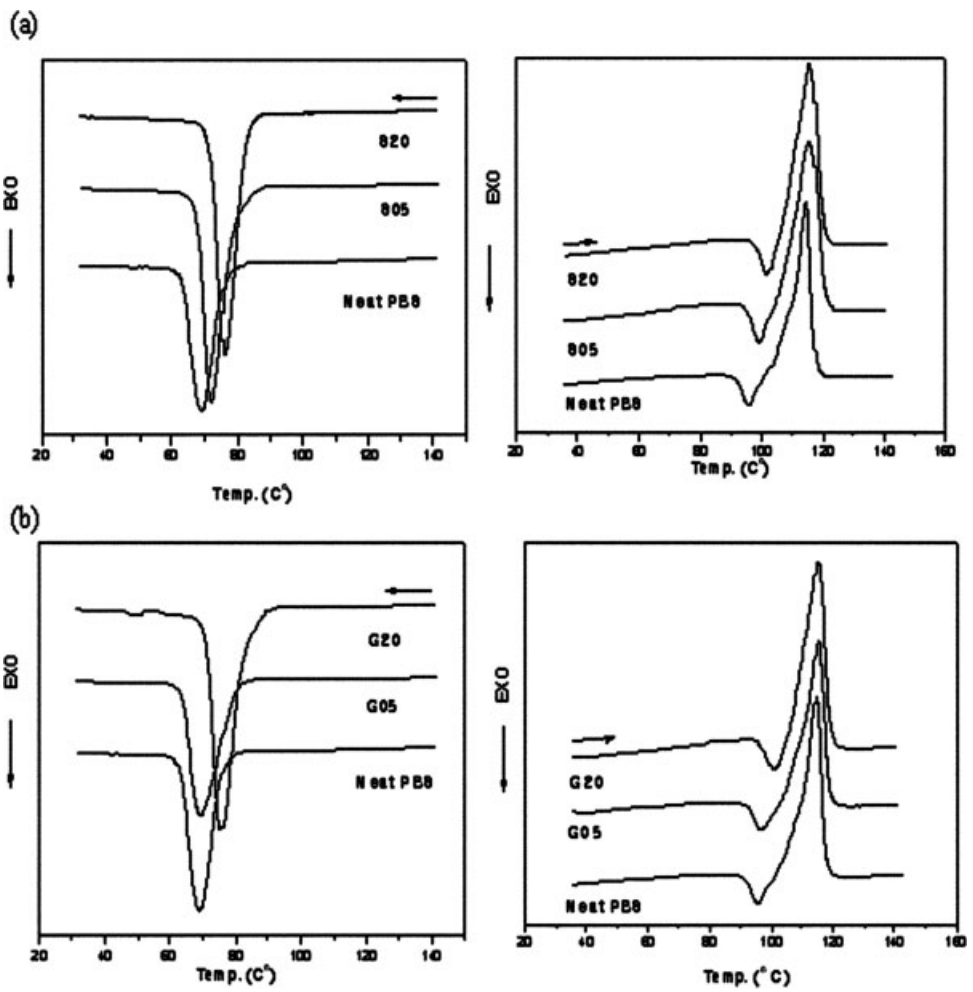

Figure 5 DSC cooling and second heating run of (a) S nanocomposites and (b) G nanocomposites.

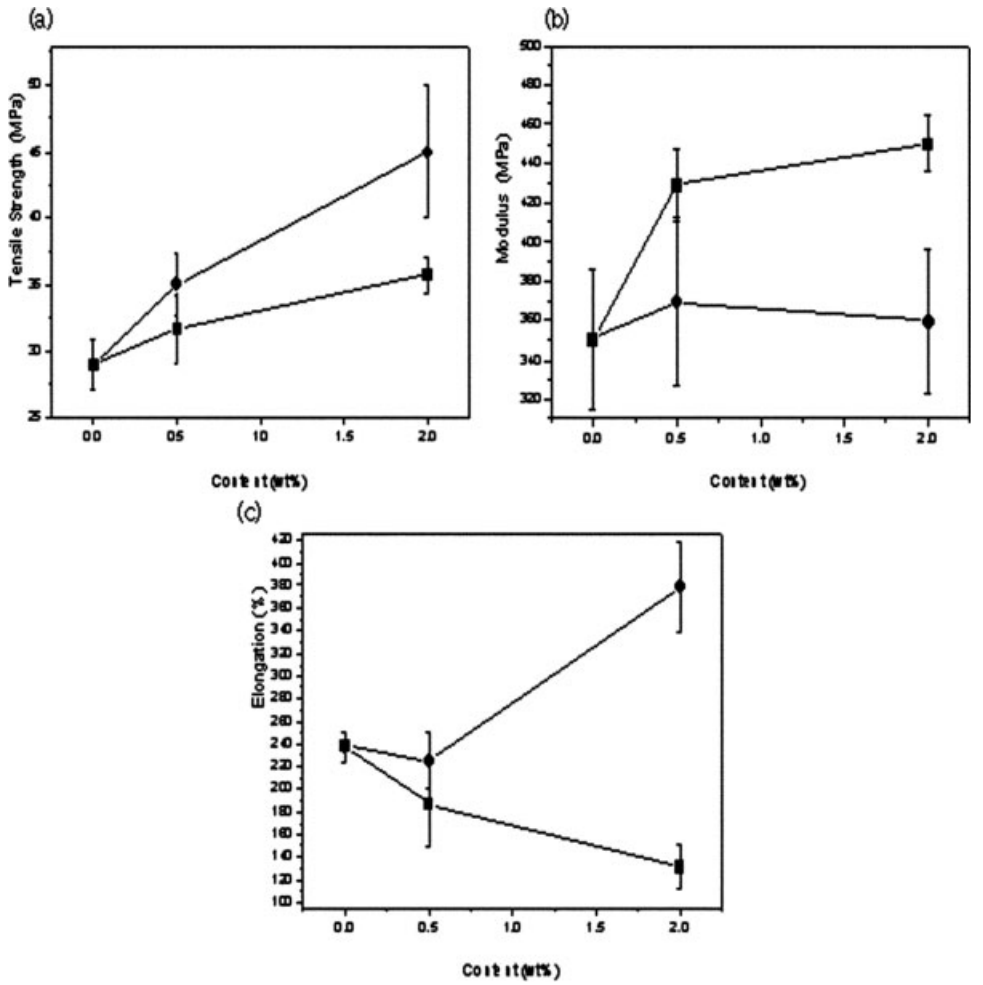

Figure 6 Mechanical properties of PBS nanocomposites: (a) tensile strength, (b) modulus, and (c) elongation at breaking.

the result is shown in Figure 4. The silica particles in the G nanocomposites are dispersed more homogeneously than the original silica particles in the S nanocomposites. In addition, the dispersed phases in the G nanocomposite are clearly smaller than those of the original silica particles in the S nanocomposites. These results indicate that the surface energy difference between silica-*g*-PBS and the PBS matrix is relatively low than original silica and PBS. That is, this can be explained that the surface of the silica-*g*-PBS is chemically similar to that of the PBS matrix. However, the surface of the original silica particles is quite different from that of PBS molecules. Based on this it can be clearly confirmed that when compared with the original silica particles, silica-*g*-PBS has much less tendency to aggregate by itself, leading to enhanced adhesion with the PBS matrix.

Thermal stability

To examine the thermal stability for the nanocomposites, TGA analysis was conducted and the results are summarized in Table II. The initial thermal degradation temperature indicating a 2% weight loss (T_D^2) was 273°C for the S and G nanocomposites, which was 9°C higher than that of neat PBS. This confirms that at the beginning of thermal decomposition, the silica particles obstruct the internal diffusion of heat because they act as insulators with a high thermal capacity. Consequently, the nanocomposites are more stable than neat PBS at the initial thermal degradation, independent of the modification of the silica particles.

On the other hand, comparing the thermal degradation temperature of 20 wt % (T_D^{20}), neat PBS, and S20 have similar values, while G20 has a value more than 20°C higher, suggesting that the modification of silica particles enhances the thermal stability of the nanocomposites. It may be likely that the dispersion of the silica particles in the PBS matrix is the main factor producing this behavior. That is, the highly dispersed silica-*g*-PBS particles in G20 act as more effective insulators than the aggregated silica particles in S20, leading to the enhanced thermal stabil-

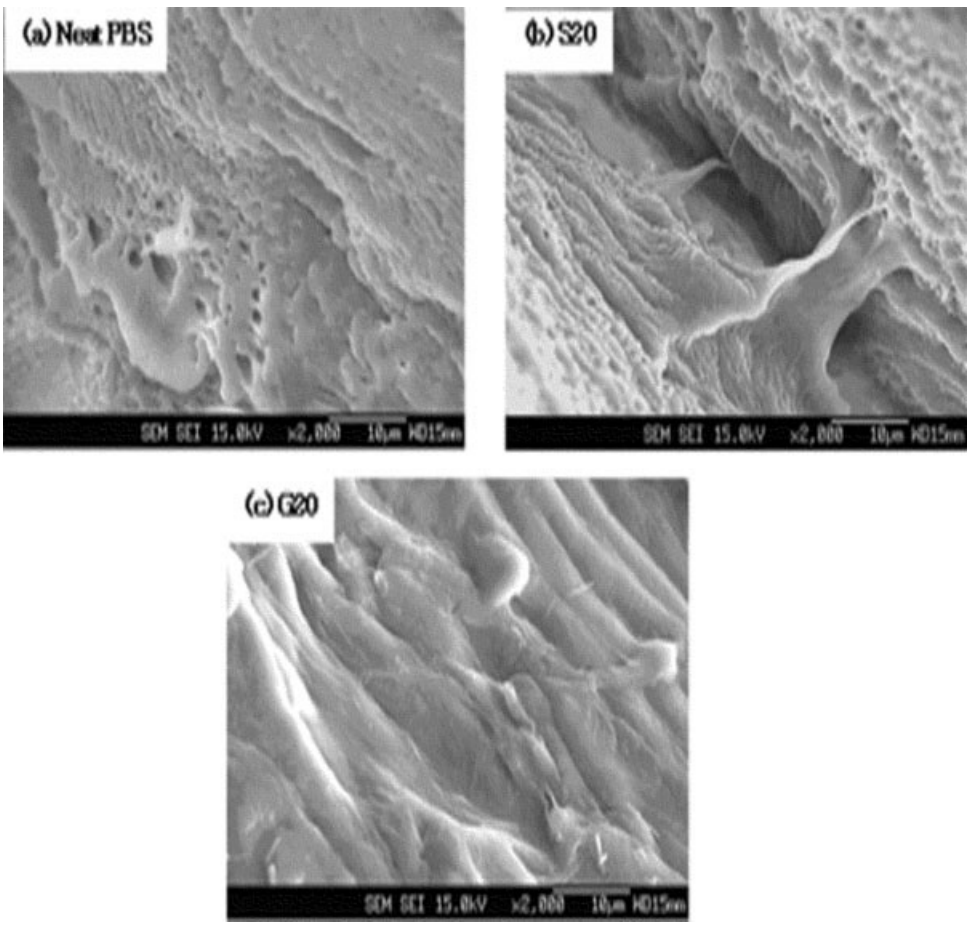

Figure 7 SEM fractographs of the tensile fractured surface.

ity. Furthermore, this result is in good agreement to TEM micrographs in Figure 4.

Thermal properties

To elucidate the thermal behavior of the neat PBS and the nanocomposites, DSC analyses were performed. The DSC thermograms for the S and G nanocomposites during the cooling and second heating scans are shown in Figure 5, and the results are summarized in Table II. Neat PBS exhibited the single cooling exothermic peak (T_c) at 69.0°C. As seen in the Figure 5 and Table II, as the silica contents increased, T_c for both S nanocomposites (original silica) and G nanocomposites (silica-*g*-PBS) shifted to the higher temperature, and their degree of supercooling ($\Delta T = T_m - T_c$) exhibited lower value than that of neat PBS. This observation can be interpreted that both the original silica and silica-*g*-PBS particles can act as nucleating agents during the crystallization process and accelerate the crystallization rates in the PBS matrix. On the other hand, relative to S nanocomposites, ΔT for the G nanocomposites showed somewhat higher values over same silica contents, confirming that the degree of the nucleating effect of silica-*g*-PBS is weaker than that of the original silica particles in the PBS matrix. This result may be attributable to the improved interfacial adhesion between the modified silica particles and PBS molecules, which induce a relatively lower nucleating effect. As for the second heating DSC curve, the melting endothermic peaks (T_m) of all of the samples were the same regardless of the modification or silica particle or its content. In summary, it can be concluded that the silica particles strongly affect the crystallization rate of PBS. That is, they contribute favorably to the faster crystallization of PBS molecules, but may not influence with the main PBS crystals.

Mechanical properties and morphology of fractured surfaces

The mechanical properties of PBS nanocomposites as a function of the contents and modification of the silica particles are shown in Figure 6. The tensile strength of the S and G nanocomposites increased with the silica content. In contrast, at the same silica

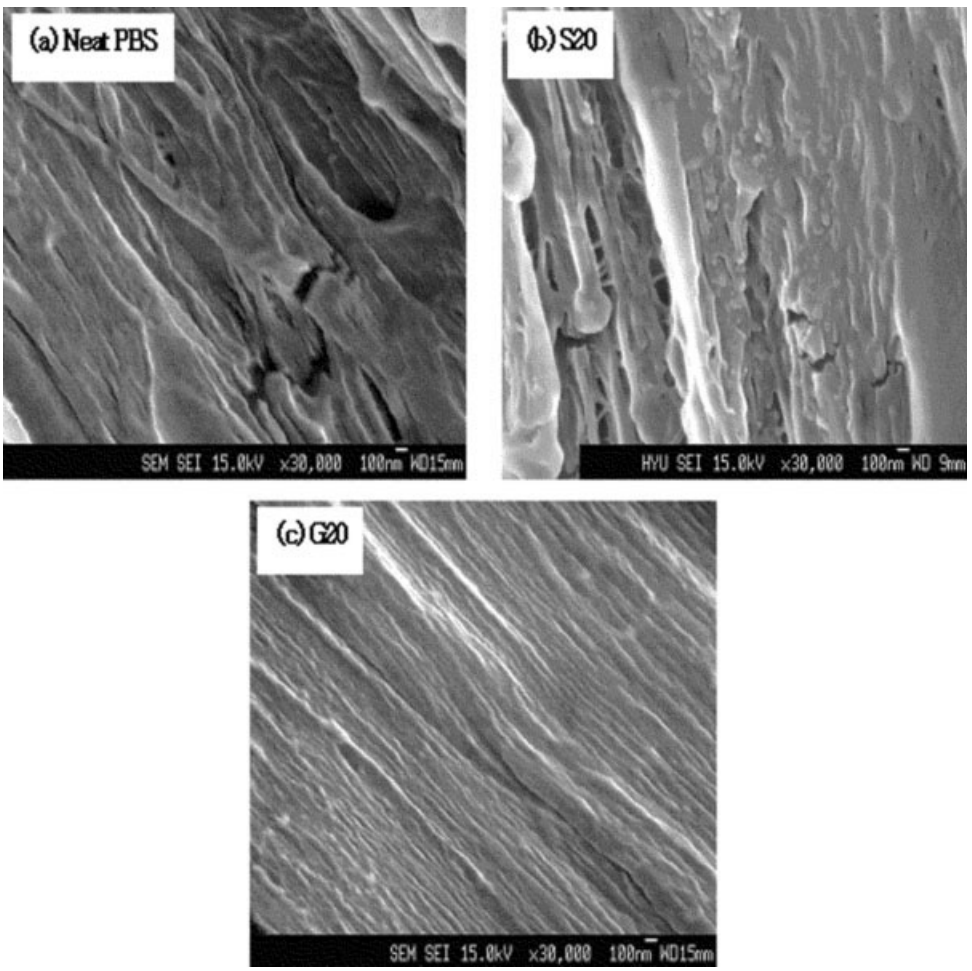

Figure 8 SEM fractographs of the horizontally fractured surface along the tensile direction.

content, the G nanocomposites filled with silica-*g*-PBS had a much greater tensile strength than the S nanocomposites, indicating that the entanglement of the grafted PBS segment with PBS molecules in the matrix occurred and this induces to the enhancement of the interfacial adhesion between the silica particles and PBS matrix.

Figure 6(b) shows the Young's modulus of the S and G nanocomposites. The Young's modulus for the S nanocomposites increased with the silica content. The high Young's modulus of the S nanocomposites may be explained that the addition of silica particles increases the stiffness. However, for G nanocomposites, a different phenomenon is observed. The Young's modulus of the G nanocomposites was increased slightly at a silica content of 0.5 wt % and remained unchanged at a silica content of 2.0 wt %. Rong et al. reported similar results for polypropylene composites filled with grafted nanoinorganic particles.[12] They suggested that the compliant layer at the interface of the grafted polymer tends to mask the stiffness of the filler particles. Therefore, the modulus of the nanocomposites containing original silica increases with the silica content, while the grafted polymer greatly decreases the stiffening effect of silica.

A remarkable difference in the nanocomposites was observed in the elongation at breaking, as shown in Figure 6(c). The elongation at breaking of the S nanocomposites decreased with the silica content, which may be due to the aggregated silica particles, as seen in Figure 4.[25] Conversely, the elongation at breaking of the G nanocomposites increased with the silica content. This result can be interpreted as follows: first, the interfacial adhesion was enhanced by the entanglement between the grafted PBS molecules and the PBS matrix. Second, the modified silica particles were well dispersed in the PBS matrix. Accordingly, G nanocomposites have a more compact structure, leading to the resistance of the crack propagation.

Scanning electron microscopy was used to observe the fractured surfaces of specimens. As Figure 7(b) shows, a coarser appearance and void formation at the interface are observed at the fractured surface of S20. In contrast, a relatively smooth surface and no

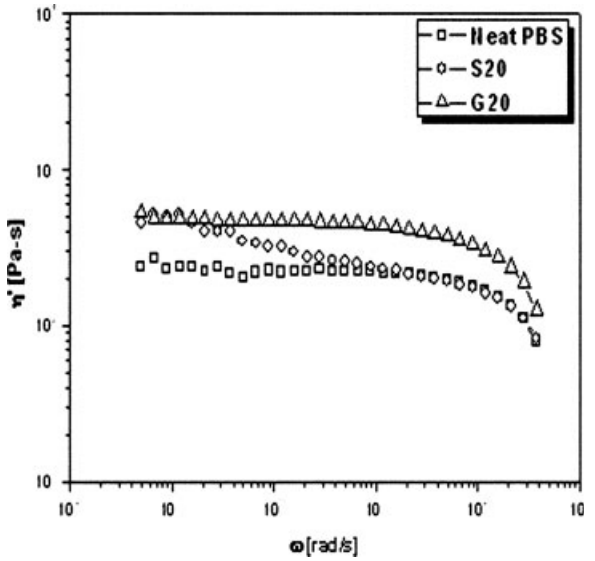

Figure 9 Dynamic melt viscosity of PBS nanocomposites.

void formation are observed at the fractured surface of G20 in Figure 7(c), supporting the results of the mechanical tests.

The elongated neck area was fractured vertically in the direction of stretching after immersion in liquid nitrogen. Comparing S20 [Fig. 8(a)] with G20 [Fig. 8(b)], numerous cracks were frequently observed in the surface of S20, indicating poor adhesion between the aggregated silica particles and PBS matrix. In contrast, the surface of G20 showed no cracks and a compactly deformed structure. This clearly suggests that the silica particles grafted with PBS molecules were dispersed homogeneously and the adhesion between the silica particles grafted with PBS molecules and PBS matrix was improved.

Rheological properties

Figure 9 shows the dynamic viscosity of the nanocomposites. S20 has a higher viscosity than neat PBS at a low frequency. This indicates that a network structure forms as a result of particle–particle interactions. As the shear force increases, all the samples exhibit the shear thinning behavior by the breakdown of the network structure. G20 has a higher viscosity than neat PBS over the entire frequency range. This may result from entanglement between the grafted PBS molecules and the PBS matrix molecules at the interface, which substantially enhances the interfacial interaction.

The storage modulus (G′) and loss modulus (G″) of the nanocomposites are displayed in Figure 10. The G′ and G″ of S20 are higher than neat PBS at low frequency. This confirms that the network structure because of the particle–particle interaction confers more elasticity than in neat PBS, and that the dissipation of energy also increases at low frequency. As the shear rate increased, the G′ and G″ of S20 showed similar value to that of neat PBS, reflecting the collapse of the network structure because of the dominant shear force.

The G′ and G″ of G20 of G20 are also higher than those of neat PBS over the entire frequency range. This suggests that grafting PBS molecules on the silica particles leads to strong entanglement with PBS molecules in the matrix. In contrast, the elastic behavior of G20 is weaker than that of S20 at low frequencies, implying that G20 does not have strong particle–particle interactions. This can be explained as follows: when the silica particles are grafted with

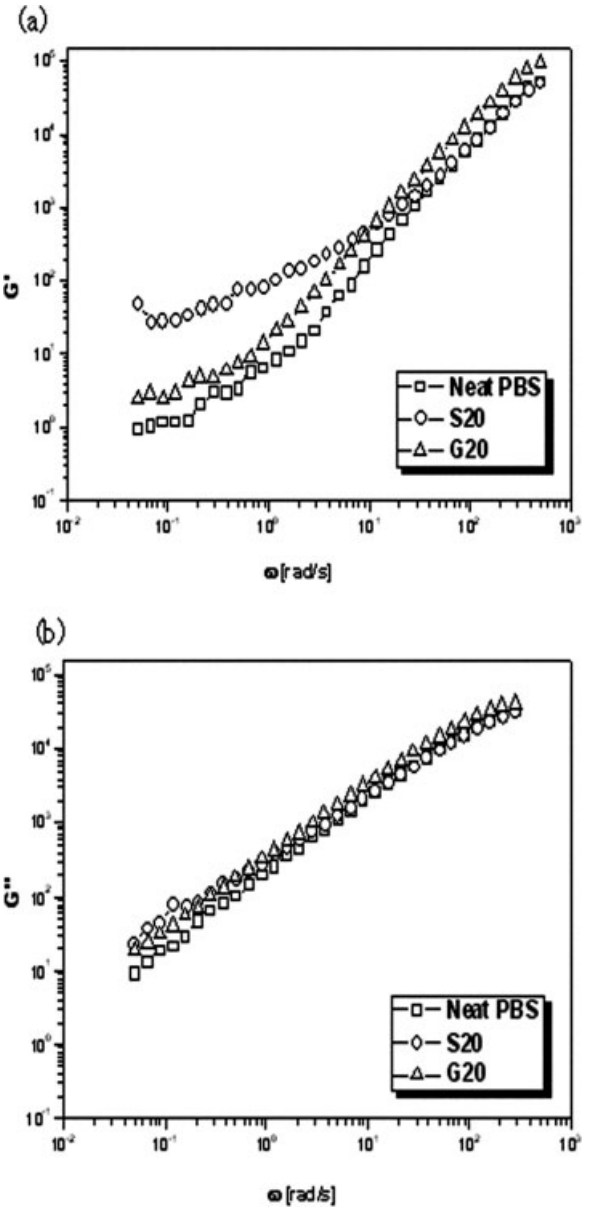

Figure 10 (a) Storage modulus (G′) and (b) loss modulus (G″) of PBS nanocomposites.

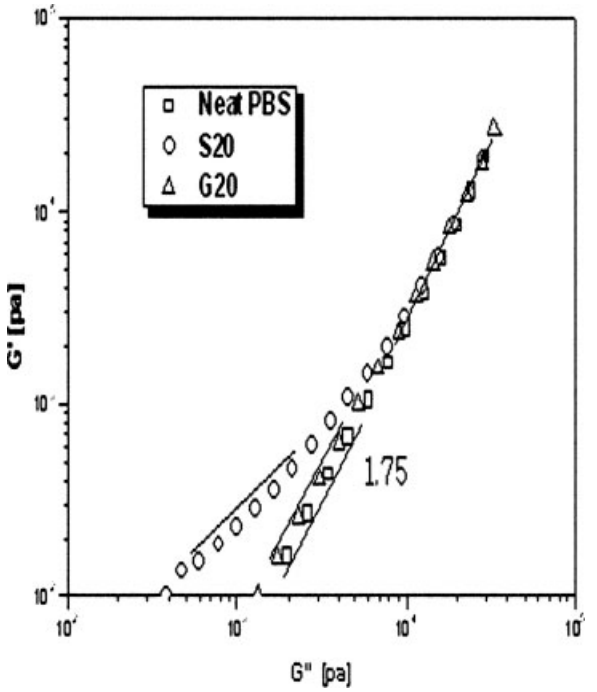

Figure 11 Cole–Cole plot for PBS nanocomposites.

PBS molecules during *in situ* polymerization, the surface energy difference between the silica particles and PBS matrix is low because the surface of the silica grafted with PBS molecules is chemically similar to that of the PBS molecules in the matrix. Therefore, the particle–particle interactions between silica are relatively weakened. As a result, the probability that can be formed as network structure becomes lower.

The Cole–Cole plot of the nanocomposites is shown in Figure 11. Neat PBS, G20, and S20 give similar master curves with slopes of 1.75, 1.64, and1.110, respectively. If the polymer melt is isotropic and homogeneous, the curve slope on the Cole–Cole plot is 2.0, irrespective of temperature.[26] Neat PBS gives a master curve with a slope of 1.75, suggesting that little interaction occurs in the molecular structure. S20 gives curves with very shallow slopes, indicating that the system of nanocomposites is heterogeneous and much energy is dissipated due to the presence of the network structures. G20 has a slightly shallower slope of 1.64 when compared with neat PBS. This is in evidence that silica-*g*-PBS has good interfacial interactions because the grafted PBS molecules mask the surface of the hydrophilic silica particles. Over the loss modulus value about 10^4, however, the slope of curves for all nanocomposites increased and approach to neat PBS curves. This result reflects that some network structure owing to particle–particle interaction (S20) and particle–matrix interaction (G20) was broken down by shear force, and becomes gradually homogeneous system.

CONCLUSIONS

Functionalized silica particles were synthesized using HDI, and PBS nanocomposites filled with silica-*g*-PBS were prepared successfully using *in situ* polymerization. Comparing the differences in the thermal, mechanical, and rheological properties of the S and G nanocomposites, the effect of grafting PBS molecules on the silica particles was investigated. Silica-*g*-PBS was well dispersed in the PBS matrix and provided good compatibility with PBS molecules, because the surface properties of the silica grafted with PBS molecules were chemically similar to those of the PBS molecules in matrix. Based on the rheology study, the S nanocomposites appeared to have a network structure due to particle–particle interactions, while the G nanocomposites showed strong adhesion between the grafted PBS molecules and PBS molecules in the matrix. Consequently, grafting PBS molecules on silica particles resulted in good dispersion and compatibility with PBS molecules in the matrix, leading to the enhanced thermal and mechanical properties when compared with neat PBS and PBS/original silica nanocomposite.

References

1. Okada, M. Prog Polym Sci 2002, 27, 87.
2. Bhari, K.; Mitomo, H.; Enjoji, T.; Yoshii, F.; Makuuchi, K. Polym Degrad Stab 1998, 62, 551.
3. Doi, Y.; Kasuya, K.; Abe, H.; Koyama, N.; Ishiwatari, S.; Takagi, K.; Yoshida, Y. Polym Degrad Stab 1996, 51, 281.
4. Yoo, E. S.; Im, S. S. Macromolecules 1995, 28, 2460.
5. Uesaka, T.; Nakane, K.; Maeda, S.; Ogihara, T.; Ogata, N. Polymer 2000, 41, 8449.
6. Fujimaki, T. Polym Degrad Stab 1998, 59, 209.
7. Sinha Ray, S.; Okamoto, K.; Okamoto, M. Macromolecules 2003, 36, 2355.
8. Giannelis, E. P. Adv Mater 1996, 8, 29.
9. Lee, W. D.; Im, S. S. Polymer 2006, 46, 1364.
10. Zhang, M. Q.; Rong, M. Z.; Friedrich, K. Handbook of Organic–Inorganic Hybrid Materials and Nanocomposites; American Scientific Publishers: California; Vol. 2, 2003, p 113.
11. Sinha Ray, S.; Bousmina, M. Polymer 2005, 46, 12430.
12. Rong, M. Z.; Zhang, M. Q.; Zheng, Y. X.; Zeng, H. M.; Walter, R.; Friedrich, K. Polymer 2001, 42, 167.
13. Zhang, M. Q.; Rong, M. Z.; Zhang, H. B.; Friedrich, K. Polym Eng Sci 2003, 43, 490.
14. Hahm, W. G.; Oh, S. G.; Im, S. S. Macromol Res 2002, 10, 221.
15. Novak, B. M. Adv Mater 1993, 5, 422.
16. Hernandez, G.; Rodriguez, R. J Non-Cryst Solids 1999, 246, 209.
17. Xu, N.; Zhou, W.; Shi, W. Polym Adv Technol 2004, 15, 654.
18. John, V.; Emily, B. Introduction to Spectroscopy, Harcourt; 2001, p 51.
19. Tsubokawa, N.; Kogure, A.; Sone, Y. J Polym Sci Polym Chem 1985, 42, 509.
20. FTIR Data Bank.
21. Lim, J. S.; Noda, I.; Im, S. S. J Polym Sci Part B Polym Phys 2006, 44, 2852.
22. Lim, J. S.; Noda, I.; Im, S. S. Polymer 2007, 48, 2745.
23. Woo, E. M.; Chiang, C. P. Polymer 2004, 45, 8415.
24. Chen, Y.; Zhou, S.; Yang, H.; Wu, L. J Appl Polym Sci 2005, 95, 1032.
25. Ahmed, S.; Jones, F. R. J Mater Sci 1990, 25, 4933.
26. Han, C. D.; Kim, J.; Kim, J. K. Macromolecules 1989, 22, 383.